Construction and Building Materials 178 (2018) 462–472

Contents lists available at ScienceDirect

Construction and Building Materials

journal homepage: www.elsevier.com/locate/conbuildmat

A constitutive numerical modelling of hybrid-based timber beams with partial composite action

T-T. Tran, V-D. Thi, M. Khelifa *, M. Oudjene, Y. Rogaume

Université de Lorraine, INRA, LERMAB, F-88 France

HIGHLIGHTS

- A numerical methodology to simulate the flexural behaviour of the hybrid timber beams was developed.
- The model was implemented as an external subroutine in Abaqus FE software.
- Comparison between experimental and numerical results is given.

ARTICLE INFO

Article history:
Received 4 November 2017
Received in revised form 29 March 2018
Accepted 8 May 2018
Available online 28 May 2018

Keywords:
Hybrid timber beams
Flexural behaviour
Orthotropic material
Isotropic hardening
Damage
Finite element model

ABSTRACT

This work focuses on the development of a three dimensional constitutive model for timber to simulate the flexural behaviour of hybrid timber-steel and timber-concrete beams. This is motivated by the lack of dedicated non linear material behaviour laws for timber in the commercial finite element software by compared to the conventional materials such as concrete and steel.

The flexural behaviour of hybrid timber beams is very complex because of the combination of the two different material behaviours and their nonlinar and partial compostion action. Numerical simulation of such behaviour requires an accurate description of the nonlinear material behaviour, in particular that of timber because of its anisotropic nature. A realistic description of the material nonlinearities and of the composite action between the different materials could aid considerably in achieving acceptable predictions. An incremental approach based on the strong coupling between orthotropic elasticity, anisotropic plasticity with mixed nonlinear isotropic hardening and an isotropic damage is used. The developed constitutive model for timber is implemented in Abaqus code using an external subroutine. The 3D FE model is calibrated and validated through comparison with experimental data reported in literature. The model is able to predict the nonlinear structural response of hybrid beams in terms of load-midspan deflection, and provides an acceptable accuracy.

1. Introduction

Timber is a structural material widely used in the engineering applications, and it is lightweight and strong. It is easier to process than steel or concrete as it requires much less energy. It is renewable, nontoxic and has a high thermal efficiency. Additionally, it is a net carbon absorber and it can be easily recycled. This environmental interest has sparked a need for a high level of knowledge of its structural behaviour, which in turn requires the characterisation of its intrinsic mechanical properties to guarantee the reliability and stability of timber structures [1].

Timber is a highly orthotropic material, and its mechanical and dimensional characteristics exhibit an exceptionally high variability with time, temperature and moisture content [2]. Tabiei and Wu [2] present a nonlinear material model with power functions to capture the stiffness change based on initial stiffness. In this work, a modified Johnson model [3] was developed to take into account the influence of strain rate on the dynamic response of timber material [2], and the parameters of the used model were adjusted to improve the fits between the predicted and the measured results.

Concerning the mechanical characterization there are a large amount of experimental studies dealing with the compressive behaviour of timber material, as reported by Reiterer and Stanzl-Tschegg [4]. These authors studied the compressive behaviour of spruce wood under uniaxial loading at different orientations with regard to the longitudinal and radial directions. The dependence of the Young modulus, Poisson ratio, crushing strength and failure mechanisms on the loading angle with respect to the grain

* Corresponding author.

https://doi.org/10.1016/j.conbuildmat.2018.05.080
0950-0618/

orientation were also addressed using a Tsai-Hill's strength criterion. For analytical analysis, the wood material is commonly assumed to be orthotropic because it presents different mechanical properties in three directions: longitudinal, tangential and radial. Nonlinear material behaviour complicates the modelling of such material, as reported by many authors [2,4,5].

A variety of elastoplastic models for timber material have been developed for the yield surface of anisotropic compressible solids. Tagarielli et al. [6] proposed an elastic-plastic constitutive model for transversely isotropic compressible solids in which a quadratic yield surface with four parameters and one hardening function has been developed. The transversely isotropic cellular solid model [6] was used to simulate the indentation test of balsa wood. Good agreement was found between the finite element results and experimental ones. By extending the Hill [7] quadratic yield criterion for incompressible solids with orthotropic symmetry, Deshpande et al. [8] developed a yield surface for compressible solids. The authors [8] applied this criterion of plasticity to analyse the behaviour of the cubic Octet truss lattice under arbitrary states of stress. The predicted results revealed that the used compressible version of the Hill [7] model, presented in [8], is not able to predict the real plastic behaviour of the Octet truss material. Schellekens and De Borest [9] applied the Hoffman model [10] to study the behaviour of plate and shell structures. In this work [9], a simpler return mapping algorithm was developed, and the calculated results are accurate for curved parts of the yield surface. To simulate the behaviour of a double shear timber steel connection, Xu et al. [11] have proposed a plastic flow law based on the Hill criterion associated to the Hoffman criterion representing the evolution of damage in wood. The obtained results [11] showed that the modelling is adequate when calibrated by the load-slip experimental response. The use a simple elastoplastic model without damage affect, describing the material degradation, cannot lead to a quite good prediction of the global load-displacement behaviour up to failure. Moreover, none of these developments are yet used in the simulation of the behaviour of hybrid timber beams with damage effect. It was the aim therefore of the present study to simulate the damage evolution in hybrid timber structures within the framework of continuum damage mechanics and plasticity.

Recent years have witnessed a renewed interest in the use of hybrid timber-steel and timber-concrete beams in high rise buildings. Indeed, the concept of combining the two materials (timber-steel and timber-concrete) has many economical and environmental advantages [12–15]. The hybrid elements can replace structural steel and concrete beams in construction, thereby allowing significant time and cost savings. The inclusion of a ductile material, in this case steel, confers to the timber-steel beam a wide range of additional advantages such as reduced creep and a high shear capacity in comparison with solid timber, which is rather poor from this point of view, and which is also prone to brittle failure. The introduction of timber material into the concrete beams reduces considerably the weight of the structures, and constitutes a major advantage where the timber is stressed by the tensile forces and the concrete by the compressive forces.

Regarding to the coupling model between orthotropic elasticity, anisotropic plasticity and an isotropic damage at different loading orientations to the grain, there is a great lack in this field. A primary motivation of this work is thus the development of a constitutive law for timber material that will allow efficient numerical solution of large structural problems subjected to various static loading conditions. The work continues the effort underway by the authors for many years to develop continuum constitutive relations to characterize a wide range of engineering applications and to validate them using the analysis of the flexural behaviour of hybrid timber beams. In the modelling, the commercial code Abaqus [16] has been used with an external subroutine, which has been implemented based on a three-dimensional constitutive model developed in this study.

2. Timber constitutive model

2.1. Theoretical aspects

The hypothesis of small deformations allows the decomposition of the total strain tensor into two additive components: elastic part $\underline{\varepsilon}^e$ and a plastic part $\underline{\varepsilon}^p$ such that:

$$\underline{\varepsilon} = \underline{\varepsilon}^e + \underline{\varepsilon}^p \tag{1}$$

The elastic strain tensor is related to the Cauchy stress tensor $\underline{\sigma}$ through elastic law [17]:

$$\underline{\sigma} = (1-D)\underline{\underline{\Lambda}} : \underline{\varepsilon}^e \tag{2}$$

where D is the isotropic damage variable; $\underline{\underline{\Lambda}}$ is the orthotropic elastic tensor of the material. The inverse has the form:

$$\underline{\varepsilon}^e = \frac{1}{(1-D)}\underline{\underline{S}} : \underline{\sigma} \tag{3}$$

$\underline{\underline{S}}$ is the elastic compliance tensor and is given in a matrix form as:

$$\underline{\underline{S}} = \underline{\underline{\Lambda}}^{-1} = \begin{bmatrix} \frac{1}{E_1} & -\frac{\nu_{21}}{E_2} & -\frac{\nu_{31}}{E_3} & 0 & 0 & 0 \\ -\frac{\nu_{12}}{E_1} & \frac{1}{E_2} & -\frac{\nu_{32}}{E_3} & 0 & 0 & 0 \\ -\frac{\nu_{13}}{E_1} & -\frac{\nu_{23}}{E_2} & \frac{1}{E_3} & 0 & 0 & 0 \\ 0 & 0 & 0 & \frac{1}{G_{12}} & 0 & 0 \\ 0 & 0 & 0 & 0 & \frac{1}{G_{13}} & 0 \\ 0 & 0 & 0 & 0 & 0 & \frac{1}{G_{23}} \end{bmatrix} \tag{4}$$

E_i is the elastic modulus in the direction (i); G_{ij} and ν_{ij} are, respectively, the shear modulus and Poisson's ratio in the plane (i-j).

The dissipative plastic potential F_p and the plastic yield criterion f can be stated as:

$$F_p = f + \frac{1}{2}\frac{1}{(1-D)}\frac{b}{Q}R^2 + \frac{S}{(1+s)}\left[\frac{Y}{S}\right]^{s+1} \tag{5}$$

$$f = \frac{\|\underline{\sigma}\| - R}{\sqrt{1-D}} - \sigma_e \tag{6}$$

with:

$$\|\underline{\sigma}\| = \sqrt{\underline{\sigma} : \underline{\underline{P}} : \underline{\sigma} + \underline{L} : \underline{\sigma}} \tag{7}$$

$$\underline{\underline{P}} = \begin{bmatrix} \alpha_{13}+\alpha_{12} & -\alpha_{12} & -\alpha_{13} & 0 & 0 & 0 \\ -\alpha_{12} & \alpha_{23}+\alpha_{12} & -\alpha_{23} & 0 & 0 & 0 \\ -\alpha_{13} & -\alpha_{23} & \alpha_{13}+\alpha_{23} & 0 & 0 & 0 \\ 0 & 0 & 0 & 3\alpha_{44} & 0 & 0 \\ 0 & 0 & 0 & 0 & 3\alpha_{55} & 0 \\ 0 & 0 & 0 & 0 & 0 & 3\alpha_{66} \end{bmatrix} \tag{8}$$

$$= [\alpha_{11} \;\; \alpha_{22} \;\; \alpha_{33} \;\; 0 \;\; 0 \;\; 0] \tag{9}$$

$$Y = \frac{1}{2}\underline{\varepsilon}^e : \underline{\sigma} + \frac{1}{2}\frac{R}{(1-D)}r = \frac{1}{2}\underline{\varepsilon}^e : \underline{\sigma} + \frac{1}{2}Qr^2; \quad R = (1-D)Qr \tag{10}$$

r represents the isotropic hardening and associated to the isotropic stress R; Q and b are the isotropic hardening parameters; σ_e is the elastic limit; Y is the force associated with the isotropic damage D; S and s are the damage parameters. $\underline{\underline{P}}$ and $\underline{L}$ are the Hoffman tensors defined in [9–11]. The constants α_{ij} are obtained using the following relationships:

$$\alpha_{12}=\alpha_{13}=\frac{\sigma_e^2}{2f_{c,0}.f_{t,0}};\quad \alpha_{23}=\sigma_e^2\left(\frac{1}{f_{c,90}.f_{t,90}}-\frac{1}{2.f_{c,0}.f_{t,0}}\right) \tag{11}$$

$$\alpha_{11}=\sigma_e^2\left(\frac{f_{c,0}-f_{t,0}}{f_{c,0}.f_{t,0}}\right);\quad \alpha_{22}=\alpha_{33}=\sigma_e^2\left(\frac{f_{c,90}-f_{t,90}}{f_{c,90}.f_{t,90}}\right) \tag{12}$$

$$\alpha_{44}=\frac{\sigma_e^2}{3f_{v,12}^2};\quad \alpha_{55}=\frac{\sigma_e^2}{3f_{v,13}^2};\quad \alpha_{66}=\frac{\sigma_e^2}{3f_{v,23}^2} \tag{13}$$

where: $f_{c,i}$ and $f_{t,i}$ are, respectively, the compressive and tension strengths in the direction (i); and $f_{v,ij}$ is the shear strength in the plane (i-j).

Using the normality rule, complementary relations are derived as follows [18]:

$$\dot{\underline{\varepsilon}}^p=\dot\lambda\frac{\partial F_p}{\partial\underline{\sigma}}=\dot\lambda\frac{\partial f}{\partial\underline{\sigma}}=\frac{\dot\lambda}{\sqrt{1-D}}\tilde{\underline{n}};\quad \tilde{\underline{n}}=\frac{1}{2}\frac{(2\underline{\underline{P}}:\underline{\sigma}+\underline{L})}{\|\underline{\sigma}\|} \tag{14}$$

$$\dot r=-\dot\lambda\frac{\partial F_p}{\partial R}=\dot\lambda\left[\frac{1}{\sqrt{1-D}}-br\right] \tag{15}$$

$$\dot D=\dot\lambda\frac{\partial F_p}{\partial Y}=\dot\lambda\left[\frac{Y}{S}\right]^s \tag{16}$$

where $\tilde{\underline{n}}$ is the normal to the loading surface; $\dot\lambda>0$ is the plastic multiplier determined using the consistency condition:

$$f=\dot f=0 \tag{17}$$

2.2. Numerical aspects

The numerical integration of the constitutive Eqs. (14–16) at the instant t_{n+1} yields:

$$\underline{\varepsilon}^p_{n+1}=\underline{\varepsilon}^p_n+\frac{\Delta\lambda}{\sqrt{1-D_{n+1}}}\tilde{\underline{n}}_{n+1} \tag{18}$$

$$r_{n+1}=r_n e^{-b\Delta\lambda}+\frac{(1-e^{-b\Delta\lambda})}{b\sqrt{1-D_{n+1}}} \tag{19}$$

$$D_{n+1}=D_n+\Delta\lambda\left[\frac{Y_{n+1}}{S}\right]^s \tag{20}$$

The plasticity criterion f_{n+1} must also satisfy the consistency condition:

$$f_{n+1}=\dot f_{n+1}=\frac{\sqrt{\underline{\sigma}_{n+1}:\underline{\underline{P}}:\underline{\sigma}_{n+1}+\underline{L}:\underline{\sigma}_{n+1}}-R_{n+1}}{\sqrt{1-D_n}}-\sigma_e=0 \tag{21}$$

Following previous methods (Chaboche and Cailletaud [18]; Simo and Hughes [19]), the number of constitutive equations to be solved can be reduced only to two:

$$f_{n+1}(\Delta\lambda,\tilde{\underline{n}}_{n+1})=\frac{\|\underline{\sigma}_{n+1}\|-R_{n+1}}{\sqrt{1-D_n}}-\sigma_e=0 \tag{22}$$

$$\underline{h}_{n+1}(\Delta\lambda,\tilde{\underline{n}}_{n+1})=2\underline{\underline{P}}:\underline{\sigma}_{n+1}+\underline{L}-2\|\underline{\sigma}_{n+1}\|\tilde{\underline{n}}_{n+1}=0 \tag{23}$$

with

$$\|\underline{\sigma}_{n+1}\|=\sqrt{\underline{\sigma}_{n+1}::\underline{\sigma}_{n+1}+:\underline{\sigma}_{n+1}} \tag{24}$$

The unknowns are the plastic multiplier $\Delta\lambda$ and the normal to the loading surface $\tilde{\underline{n}}_{n+1}$ are obtained by solving iteratively the Eqs. ((22) and (23)) using the Newton-Raphson scheme [19].

2.3. Local integration algorithm

To obtain the unknown quantities $\underline{\sigma}_{n+1}$, R_{n+1} and Y_{n+1}, the numerical integration of the coupled constitutive equations is performed out using the radial return algorithm proposed by Simo and Hughes [20]. This algorithm splits the integration procedure into two parts: a damaged elastic prediction affected by the previous damage value, and a damaged plastic corrector which includes both the damaged elastic relation and the damaged plastic consistency condition.

Knowing the total increment of strain $\Delta\underline{\varepsilon}$ at the instant t_{n+1}, the quantities $\underline{\sigma}_{n+1}$, R_{n+1} and Y_{n+1} are then obtained.

(i). Elastic prediction

At time t_{n+1} the response is assumed elastic, and the trial stress $\underline{\sigma}^*_{n+1}$ is obtained as:

$$\underline{\sigma}^*_{n+1}=\underline{\sigma}_n+(1-D_n)\underline{\underline{\Lambda}}:\Delta\underline{\varepsilon} \tag{25}$$

Substituting the value of $\underline{\sigma}^*_{n+1}$ in the expression of the criterion f_{n+1} results in

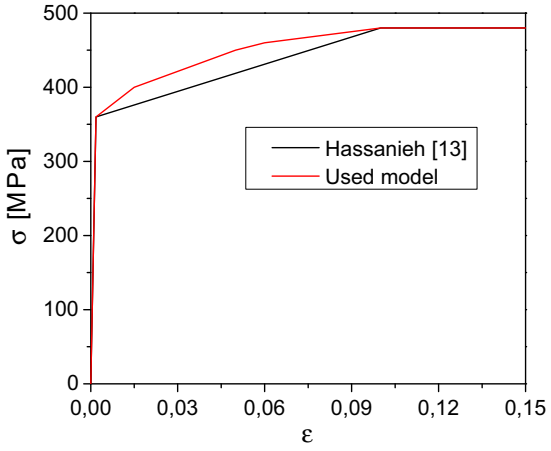

Fig. 2. Stress–strain relationship for the steel I-profile.

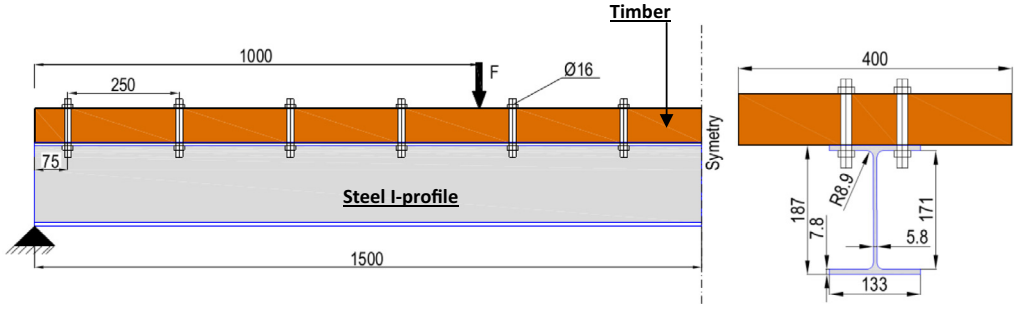

Fig. 1. Geometry of the studied specimens (dimensions in [mm]).

$$f_{n+1} = \frac{\|\underline{\sigma}^*_{n+1}\| - R_n}{\sqrt{1-D_n}} - \sigma_e \quad \text{and} \quad \|\underline{\sigma}^*_{n+1}\| = \sqrt{\underline{\sigma}^*_{n+1} : \underline{\underline{H}} : \underline{\sigma}^*_{n+1} + \underline{L} : \underline{\sigma}^*_{n+1}} \tag{26}$$

If $f_{n+1} < 0$, the solution is purely elastic, and the unknown quantities at the instant t_{n+1} are obtained as:

$$\underline{\sigma}_{n+1} = \underline{\sigma}^*_{n+1}; R_{n+1} = R_n = 0 \quad \text{and} \quad Y_{n+1} = Y_n = 0 \tag{27}$$

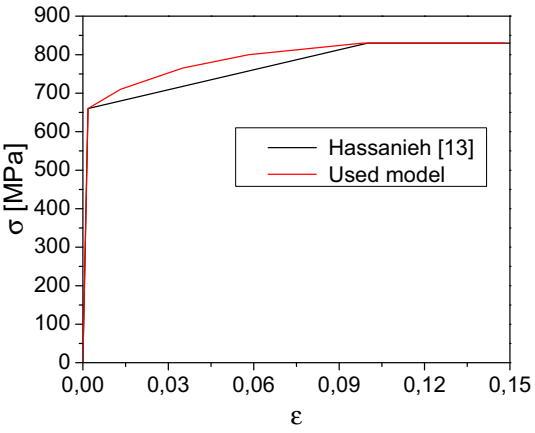

Fig. 3. Stress–strain relationship for the bolt.

(ii). Radial correction

However, if $f_{n+1} \geqslant 0$, the Newton–Raphson scheme is used to obtain the unknowns parameters $\Delta\lambda$ and $\underline{\tilde{n}}_{n+1}$ of Eqs. (22) and (23).

Successive corrections are used to ensure Eqs. (22) and (23) are equal to zero, which results in updated values of the unknowns $\Delta\lambda$ and $\underline{\tilde{n}}_{n+1}$ at instant t_{n+1}:

$$f_{n+1} = \frac{\|\underline{\sigma}_{n+1}\| - R_{n+1}}{\sqrt{1-D_n}} - \sigma_e = 0; \quad \|\underline{\sigma}_{n+1}\| = \sqrt{\underline{\sigma}_{n+1} : \underline{\underline{P}} : \underline{\sigma}_{n+1} + \underline{L} : \underline{\sigma}_{n+1}} \tag{28}$$

$$\underline{h}_{n+1} = 2\underline{\underline{P}} : \underline{\sigma}_{n+1} + \underline{L} - 2\|\underline{\sigma}_{n+1}\|\underline{\tilde{n}}_{n+1} = 0 \tag{29}$$

Once the iterative scheme has converged, the following quantities are updated:

$$\underline{\sigma}_{n+1} = \underline{\sigma}^*_{n+1} - (1-D_n)\underline{\underline{\Lambda}} : \Delta\underline{\varepsilon}^p = \underline{\sigma}^*_{n+1} - \Delta\lambda\sqrt{1-D_n}\underline{\underline{\Lambda}} : \underline{\tilde{n}}_{n+1} \tag{30}$$

$$R_{n+1} = Q(1-D_n)r_{n+1} = Q(1-D_n)\left(r_n e^{-b\Delta\lambda} + \frac{1-e^{-b\Delta\lambda}}{b\sqrt{1-D_n}}\right) \tag{31}$$

$$Y_{n+1} = \frac{1}{2}\frac{\underline{\sigma}_n : \underline{\underline{\Lambda}}^{-1} : \underline{\sigma}_n}{(1-D_n)^2} + \frac{1}{2}\left(\Delta\underline{\varepsilon} - \Delta\lambda\frac{\underline{\tilde{n}}_{n+1}}{\sqrt{1-D_n}}\right) : \underline{\underline{\Lambda}} : \left(\Delta\underline{\varepsilon} - \Delta\lambda\frac{\underline{\tilde{n}}_{n+1}}{\sqrt{1-D_n}}\right) + \frac{\underline{\sigma}_n}{(1-D_n)} : \left(\Delta\underline{\varepsilon} - \Delta\lambda\frac{\underline{\tilde{n}}_{n+1}}{\sqrt{1-D_n}}\right) + \frac{Q}{2}\left[r_n e^{-b\Delta\lambda} + \frac{(1-e^{-b\Delta\lambda})}{b\sqrt{1-D_n}}\right]^2 \tag{32}$$

Table 1
Mechanical properties of the LVL.

Elasticity	Plasticity	Damage
E_1 = 13000 MPa; E_2 = 430 MPa $\nu_{12} = \nu_{13}$ = 0.41; ν_{23} = 0.33. $G_{12} = G_{13}$ = 800 MPa; G_{23} = 125 MPa	Q = 10 MPa; b = 2.5; σ_e = 35 MPa; $f_{c,0}$ = 23 MPa; $f_{c,90}$ = 2.8 MPa; $f_{t,0}$ = 21 MPa; $f_{t,90}$ = 0.4 MPa; $f_{v,12} = f_{v,13} = f_{v,23}$ = 3MPa;	S = 0.45 MPa; s = 1.2

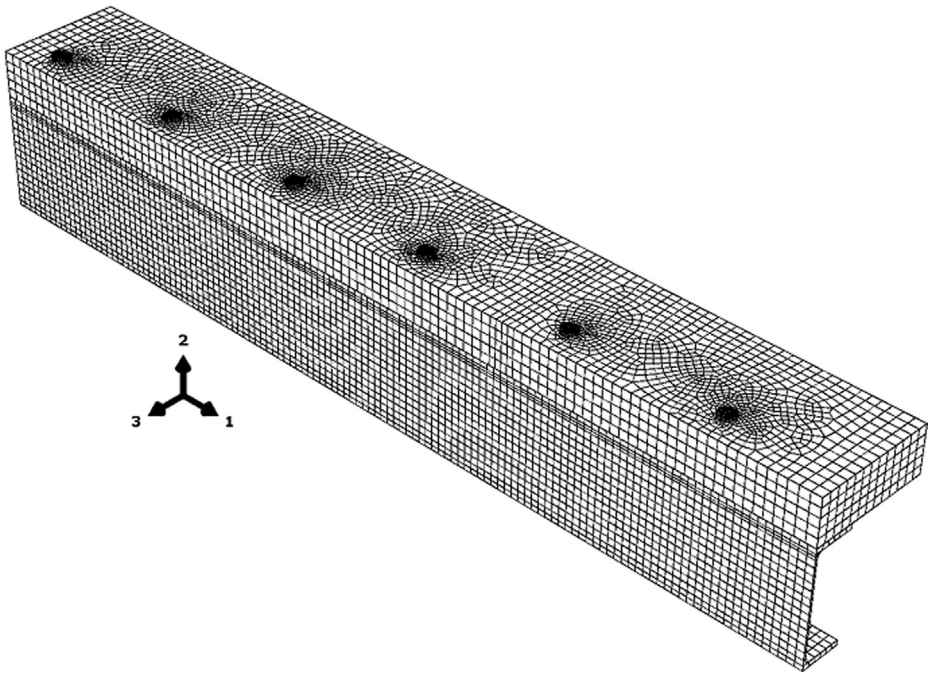

Fig. 4. FE Model of the studied timber-steel hybrid beam (one quarter).

2.4. Identification procedure

The material parameters (elasticity, plasticity and damage) were determined using a combination of numerical simulations and experimental data obtained with bending tests.

(i). Elastic parameters

Timber material is highly orthotropic and requires a large number of properties for its characterization including in the elastic domain. Nonetheless, it was assumed that the behaviour in the radial direction (2) is similar to that observed in the transverse direction (3) to the rings, which

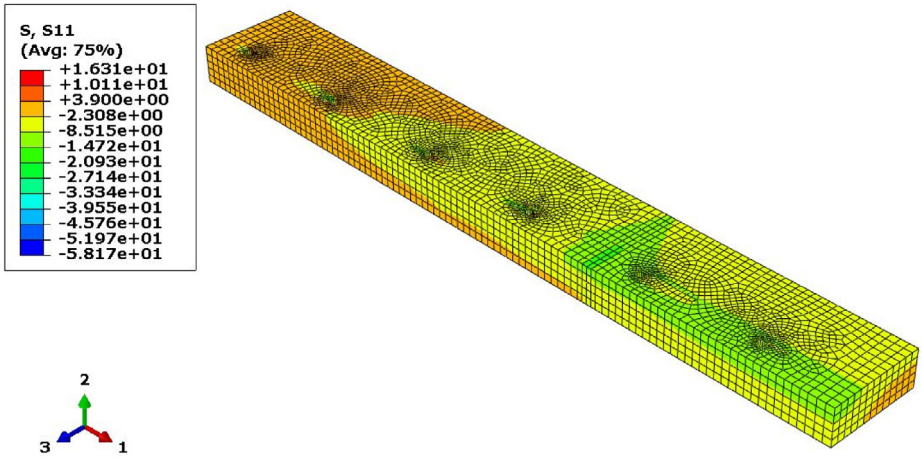

(a). v=10.7mm

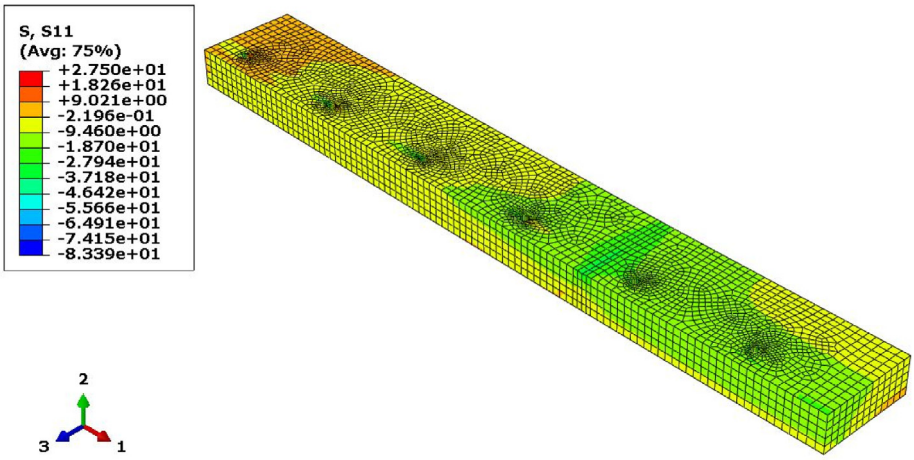

(b). v=24.84mm

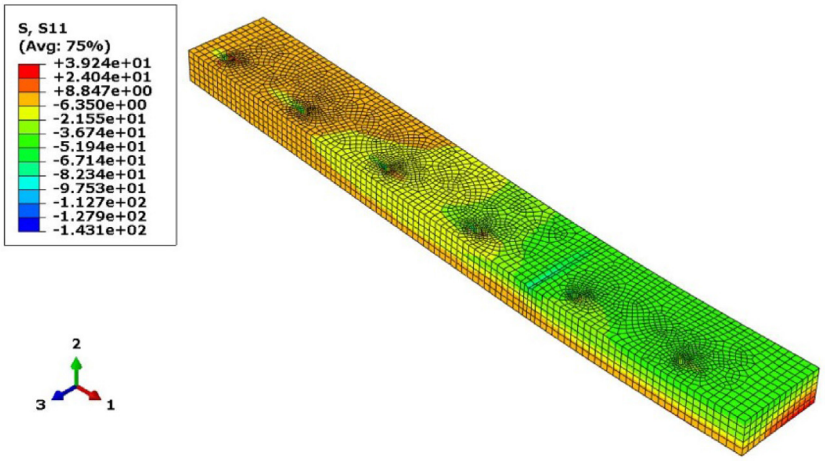

(c). v=123.7mm

Fig. 5. Contours of the longitudinal stress σ_L at different deflection levels (timber part only).

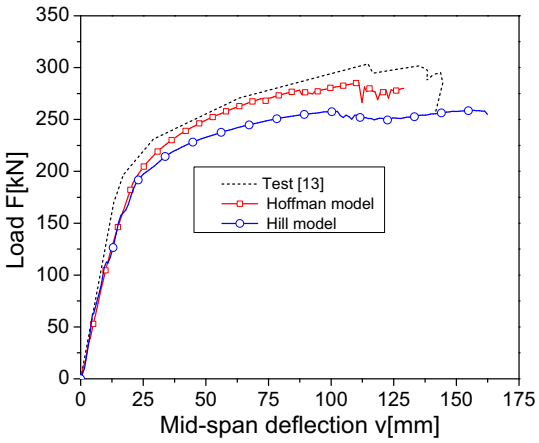

Fig. 6. Load versus mid-span deflection response for the timber-steel hybrid beam.

translates into: $E_2 = E_3$, $\nu_{12} = \nu_{13}$, $G_{12} = G_{13}$. The same assumption is used by many authors as reported by Reiterer and Stanzl-Tschegg (2001) in ref [4].

- In bending tests, where the beam is primarily stressed in the longitudinal (grain) direction (1), it is probable that the modulus E_1 is the more important parameter. The elastic modulus E_1 is calculated only in the elastic linear part of the load-displacement curves.
- Knowing E_1, the other elastic proprieties are estimated from the standards of practice defined in EC5. For example, if $E_1 = 13000$ MPa, the wood used was C35 class, for which the characteristics ($E_1 = E_0$; $E_2 = E_{90}$; G_{23}; $G_{12} = G_{13}$) are known.

(ii). Plastic parameters

The material parameters for the plasticity (σ_e, Q, b and α_{ii}) were determined from the non-linear part of the load-displacement experimental data curve.

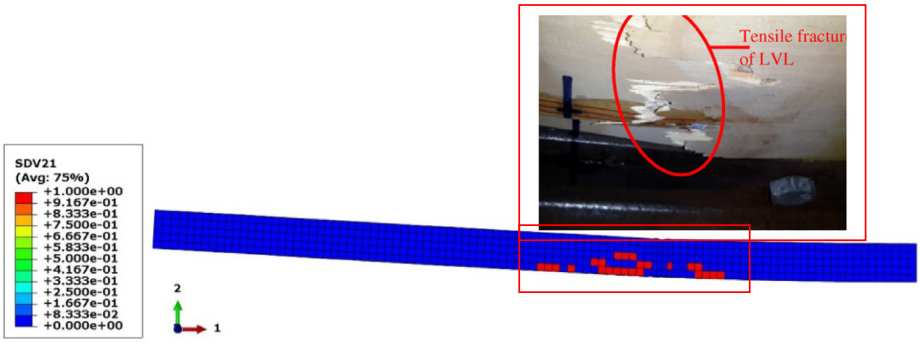

(a). Numerical and experimental [13] failure modes in LVL panel

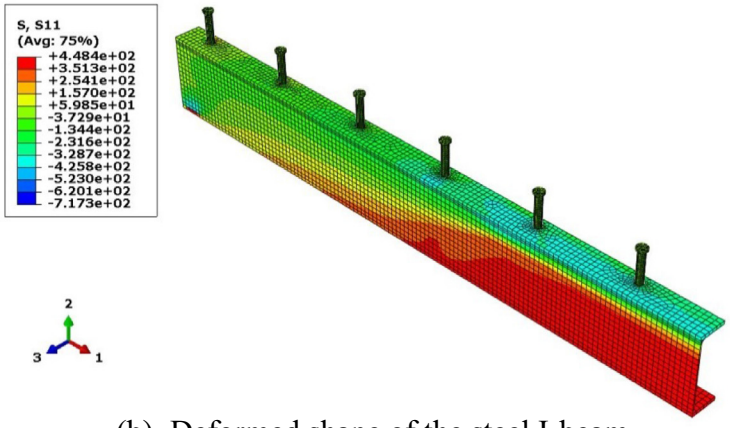

(b). Deformed shape of the steel I-beam

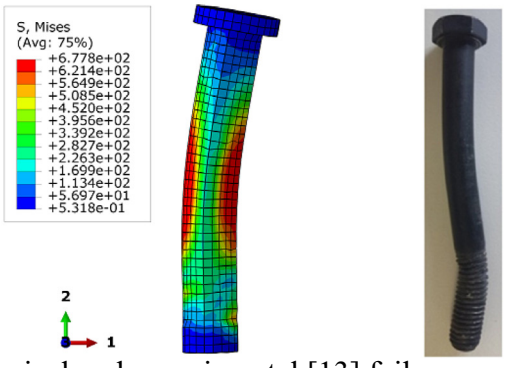

(c). Numerical and experimental [13] failure modes of the fasteners

Fig. 7. Comparison between predicted and experimental ruptures.

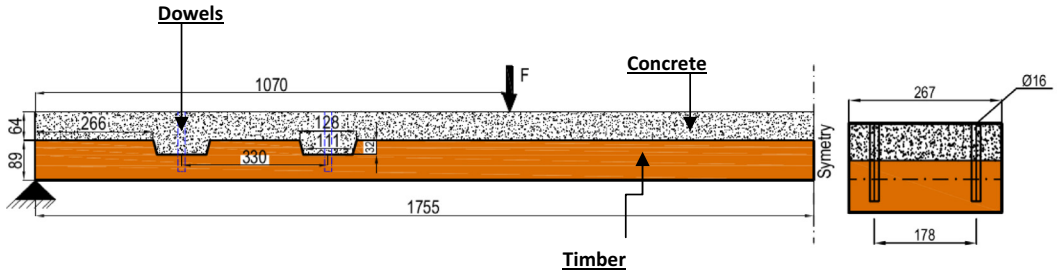

Fig. 8. Four-point bending test of timber-concrete hybrid beam (dimensions in [mm]).

Table 2
Mechanical properties for Spruce wood.

Elasticity	Plasticity	Damage
E_1 = 11000 MPa; E_2 = 340 MPa $\nu_{12} = \nu_{13}$ = 0.41; ν_{23} = 0.33. $G_{12} = G_{13}$ = 650 MPa; G_{23}=110 MPa.	Q = 11 MPa; b = 2.3; σ_e = 24 MPa σ_e; $f_{c,0}$ = 21 MPa; $f_{c,90}$ = 2.5 MPa; $f_{t,0}$ = 13 MPa; $f_{t,90}$ = 0.3 MPa; $f_{v,12} = f_{v,13} = f_{v,23}$ = 2.7 MPa;	S = 0.15 MPa; s = 1.2

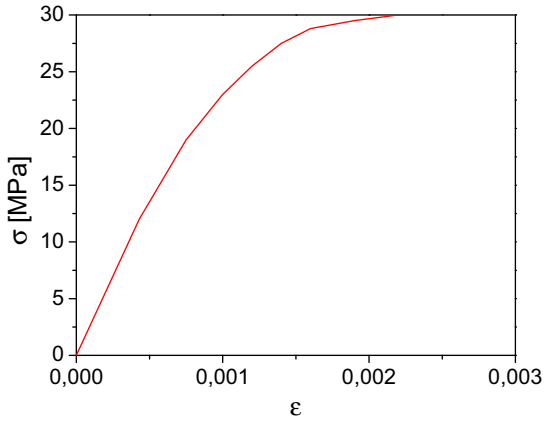

Fig. 9. Stress–strain relationship for the concrete material.

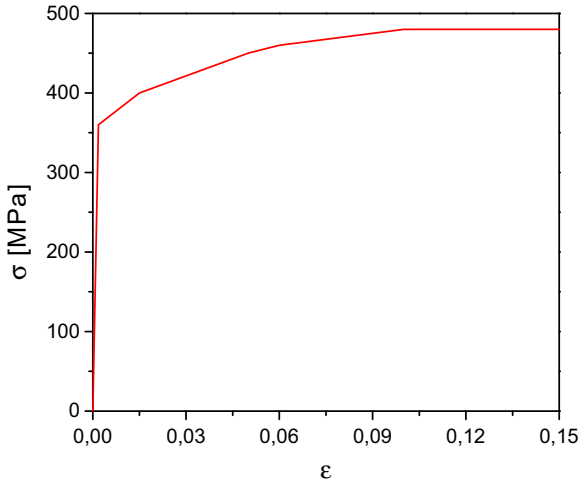

Fig. 10. Stress–strain relationship for the steel dowel.

- σ_e is assumed to be equal to the flexural strength value $f_{m,k}$. According to EC5, for the average value found for the modulus of elasticity along the longitudinal direction $E_1 \approx 14$ GPa, the characteristic value for strength in bending (for C35) is $f_{m,k} = \sigma_e = 35$ MPa .
- Q and b are the non-linear isotropic hardening parameters. The agreement between Q and b derived from experimental and numerical results confirm that the modelling is working well.
- Knowing the wood class C35, for which the characteristics ($f_{c,i}$ and $f_{t,i}$ are the compressive and tension strengths in the direction (i); and fv,ij is the shear strength in the plane (i-j)) are known, the parameters α_{ii} are calculated using the relationships (Eqs. (11) to (13)).

(iii). Damage parameters: the damage can be described by only two parameters (S and s)
. In Eq. (20), the parameter S account for the ductility of the material, and the exponent s is used to accelerate or delay the occurrence of damage.

- Parameters S and s are obtained by constraining the coupled constitutive equations associated to the Hoffman yield criterion to reproduce the experimental data. They are calculated from the nonlinear part of the measured values, and where the damage was assumed to occur when a quadratic stress function involving the nominal stress ratios reached unity.
- Due to the difficulty to obtain better values of S and s, they were chosen to be equal to those used in simulations, where the numerical response can be controlled by the user and can be stopped at the desired time, which is the reason why the computed ultimate load for the two examples is almost identical to the experimental one.

It is worth noting that the material properties of FE models, used in simulations, are slightly adjusted in order to approach the experimental results. For further details on the identification procedure of mechanical constants of plasticity models by using the yield stress and the coefficients of plastic anisotropy, the references [4,5,11] are recommended.

3. Validation of the timber constitutive model

The validation of the 3D finite element model of the flexural behaviour of hybrid timber-steel and timber-concrete beams is analysed using experimental data presented by Hassanieh [13] and Gutkowski [14] with respect to the load-carrying capacity and the failure pattern.

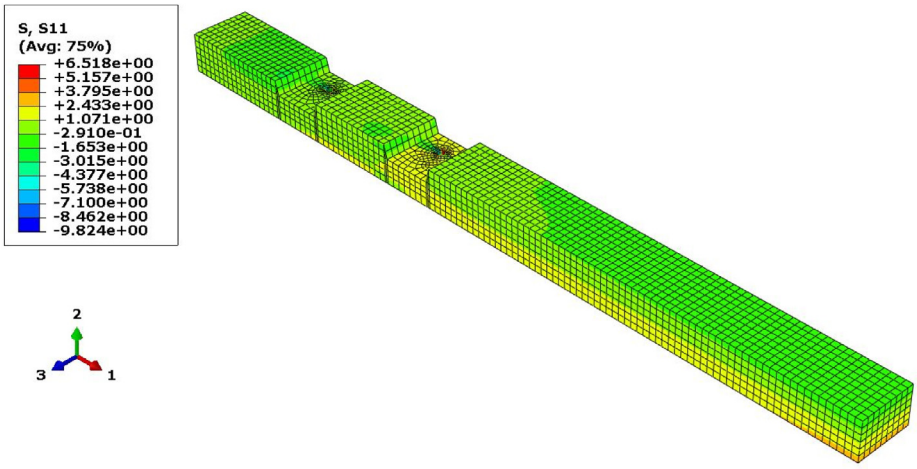

(a). v=5.02mm

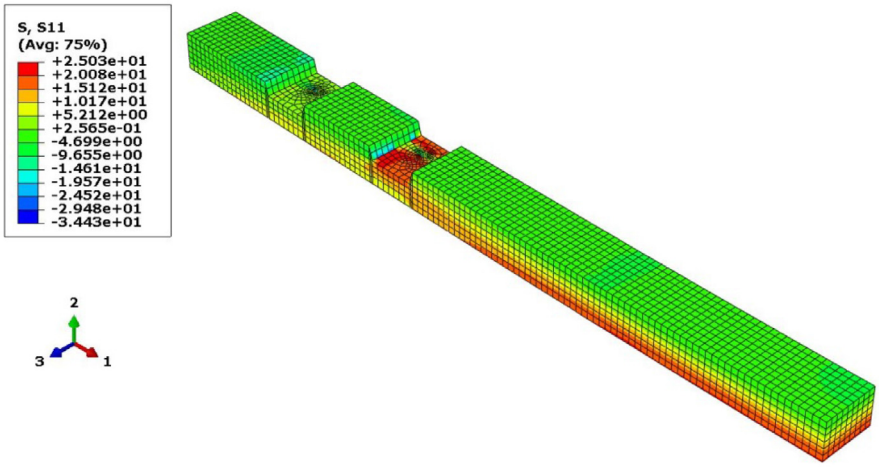

(b). v=41.11mm

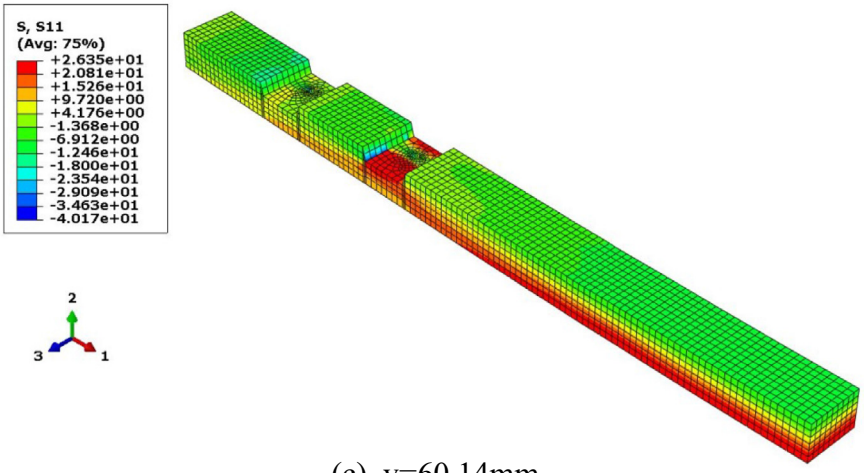

(c). v=60.14mm

Fig. 11. Distribution of the longitudinal normal stress σ_L in the timber part.

3.1. Timber-steel hybrid beams in bending

An experimental program consisting of four-point bending tests on timber-steel hybrid beams was carried out by Hassanieh et al. [13]. For reasons of symmetry in both geometry and loading, only a half of the hybrid beam was shown in Fig. 1.

The laminated veneer lumber (LVL) panel had the following geometrical characteristics: 75 mm thick, 400 mm width and 3 m long [13]. LVL panel was formed by bonding Radiata Pine laminated veneers using Phenolic adhesives with respect to the AS/NZS 2098 [21] specifications.

The steel I-profile used for the manufacture of the timber-steel hybrid specimen was Australian 200UB25.4 [13]. The dimensional characteristics and the mechanical properties of this cross-section comply with the specifications of AS/NZS 3679.1 [22].

The model adopted here assumed the following:

- the cross-sections remained planar after deformation;
- there was no slipping between the adhesive and the adjacent timber lamellas, and at an interface between the steel I-profile and LVL beam;
- the stress–strain relationship for the steel I-profile was elasto-plastic (Fig. 2);
- the stress–strain relationship for the bolt is shown in Fig. 3.

The mechanical properties of the LVL are recapitulated in Table 1. The other parameters, such as the average initial density, and the moisture content, are, respectively, taken equal to ρ_0 = 570 kg/m^3 and ω = 12%.

In simulations, only a quarter of the hybrid beam was modelled using a C3D8R element as shown in Fig. 4. The finite element (FE) mesh consisted of 20,424 brick elements (14835 for the LVL, 3913 for the steel I-profile, and 1676 for the bolts) type C3D8R with reduced integration. Contact between all the components, timber, I-beam and bolts, was modelled using Coulomb's friction law with a coefficient μ = 0.21.

Fig. 5 shows the evolution of the longitudinal stress σ_L, of the LVL panel only, for different vertical displacements. As expected, the isobars show the top fibres of the timber part are in compression. The σ_L starts to decrease by the quick formation of a macroscopic crack in timber which starts at the contact interface of the two parts of the hybrid beam at a vertical displacement of about 123.7 mm. The rupture initiated from the lower wood fibres and propagated to the top.

The load versus mid-span deflection of the timber-steel hybrid beam predicted by the Hill and Hoffman FE models are compared with the measured results in Fig. 6. The response obtained by the Hoffman model is linear up to a vertical displacement of v = 5.3 mm, corresponding to an applied load F = 52.3 kN. Then, the response becomes nonlinear up to a maximum displacement of v = 110.53 mm, corresponding to a maximum force F = 286.56 kN. Beyond this displacement, the build-up of damage in the elements of timber part within the contact zones causes the applied force to drop slightly to F = 264.86 kN. At the displacement v = 110.53 mm, the differences between experimental and predicted ultimate loads are about 16.2% and 5.0%, respectively, for the Hill and Hoffmann. Fig. 6 shows clearly that the predicted values using the Hoffman model are very close to the measured values, compared to those obtained by the Hill model.

Fig. 7 show a comparison between the numerical failure and the experimental one. It can be seen that the model correctly predicts the damaged zones. The crack initiated from the contact zone (in the lower wood fibres region) and propagated upwards through the wood (Fig. 7a). The stress fields observed on the steel I-beam and the bolts at the time of failure are, respectively, illustrated in Fig. 7b and c. The bolts are subject to higher stresses (675 MPa) than the steel I-beam (448 MPa), and they deform plastically as shown in Fig. 7c.

3.2. Timber-concrete hybrid beams in flexure

The previously developed FE model was also used to simulate the four-point bending test of the timber-concrete hybrid beam performed by Gutkowski R. et al. [14]. The specimen geometry and boundary conditions are shown in Fig. 8. The wood density and the moisture content were taken as ρ = 460 kg/m^3 and ω = 12%. The wood specimen was of the Spruce Pine-Fir species group, as reported in [14]. The material properties of the used timber are listed in Table 2.

The used stress–strain relationships in simulations for the concrete material under uni-axial compression and the steel dowel are, respectively, given in Figs. 9 and 10.

A quarter of the timber-concrete hybrid beam was modelled using a C3D8R element. The FE model consisted of 7206 elements for the timber panel, 3166 elements for the concrete part and 1032 elements for the steel dowels. Contact between all the components, wood, concrete and dowels, was modelled using Coulomb's friction law, and the friction coefficient was assumed μ = 0.23.

Fig. 11 show the longitudinal stress contours at different mid-span deflections. It can be seen that the timber specimen shows a typical stress distribution of a homogenous beam, where the neutral axis is clearly visible and the lower fibres are submitted to tensile forces. The longitudinal normal stress σ_L increases with the increase of the vertical displacement. Accordingly, the maximum of normal stress (σ_L = 40.17 MPa at a displacement of v = 60.14 mm) is observed at the extreme tensioned fibres and around the locations of the dowel connectors.

The overall responses, i.e. the load-deflection curves, predicted by the proposed model, are compared with the measured values performed by Gutkowski R. et al. [14] and shown in the Fig. 12. Numerical results obtained using the two models (Hill and Hoffman) are similar until a vertical displacement v = 54.72 mm (F = 24.8 kN). The response given by Hoffman model is linear up to a displacement v = 6.1 mm, corresponding to an applied load F = 3.51 kN. Then, the response becomes nonlinear up to a maximum displacement v = 70.1 mm, corresponding to a maximum load F = 28.22 kN. Beyond this limit, the initiation of the damage in the timber specimen around the locations of the dowels causes the applied force to drop abruptly to F = 7.73 kN (v = 78.1 mm).

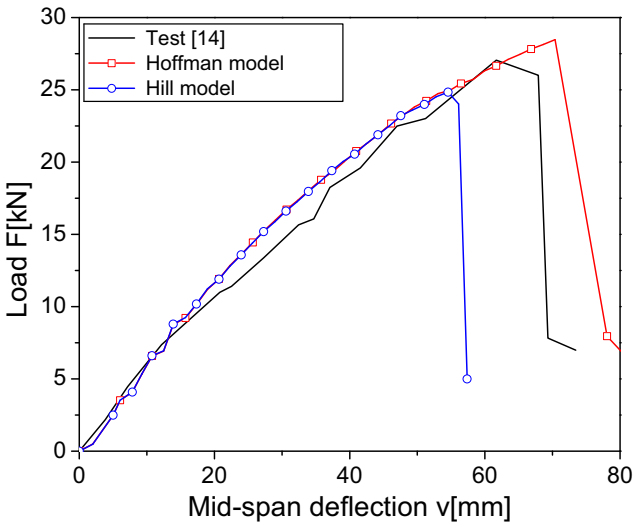

Fig. 12. Load versus mid-span deflection curves of timber-concrete beam in flexure.

Fig. 13 shows a comparison between numerical and experimental cracks. It can be seen that the failure initiates in the tensile zone around the location of dowels, and propagated to the lower fibres zone. In the crack zones, the damage variable reaches the maximum value (D = SDV21 = 1), the stresses decrease to zero ($\sigma = 0$), and the corresponding finite element becomes inactive and completely damaged (Fig. 13b).

The results obtained for the two simulated examples showed that the developed 3D FE model offer aceptable predictions of the flexural behaviour of hybrid timber-steel and timber-concrete beams, and to predict where the cracks can appear in the timber samples during bending tests.

4. Conclusion

In this paper, a nonlinear 3D orthotropic material model based on the Hoffman criterion for timber material was presented, and applied to the analysis of the flexural behaviour of hybrid timber beams. The proposed nonlinear constitutive model for timber material was very suitable for 3D incremental approaches used by the finite element software. A local approach, based on the coupling between orthotropic elastic, anisotropic plastic behaviour with isotropic hardening, and isotropic ductile damage, was developed. The mathematical formulation and the numerical aspects of

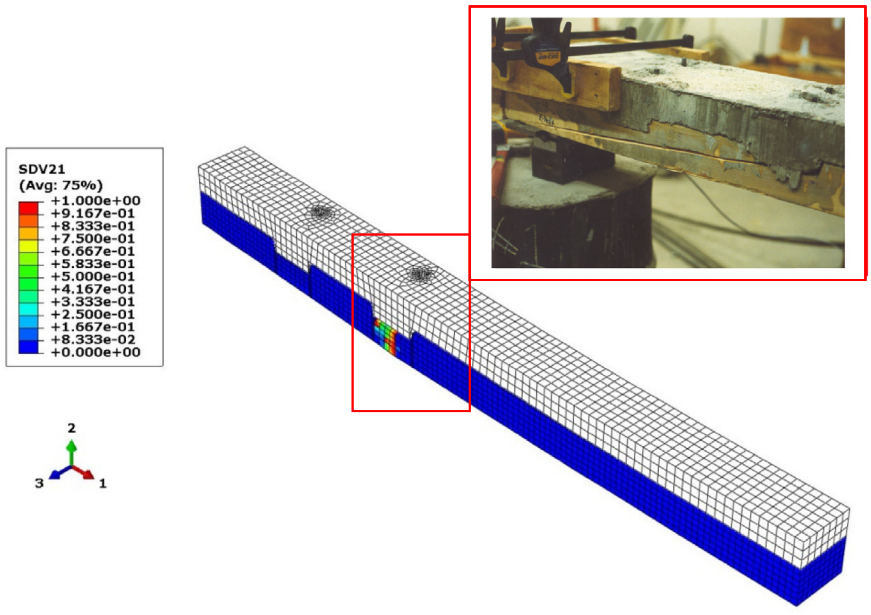

(a). Numerical and experimental [14] failure modes

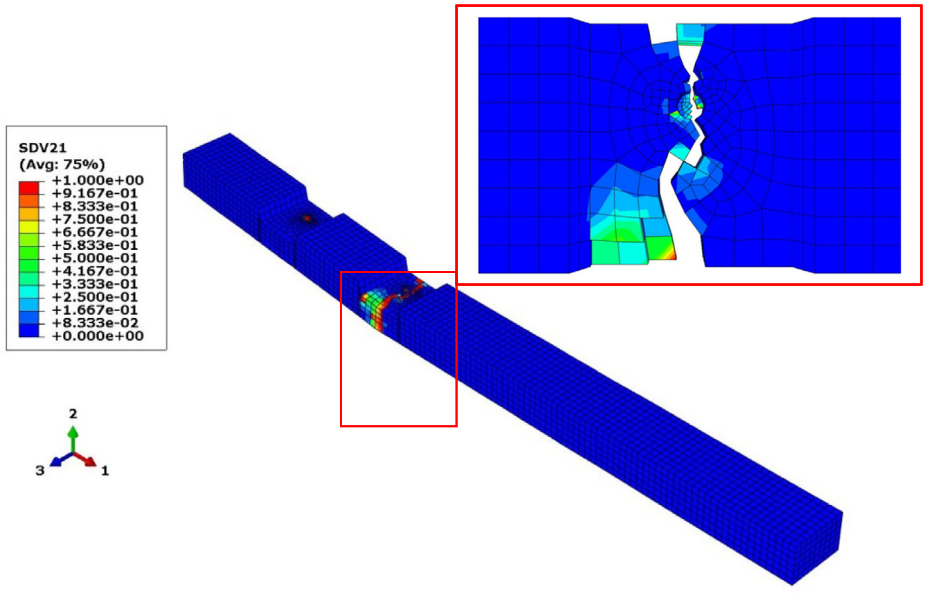

(b). Failure modes of the timber part

Fig. 13. Failure modes of timber-concrete beam in flexure.

the 3D FE model, implemented in the Abaqus code using an external subroutine, are presented in detail.

Two bending tests of hybrid timber beams, published in literature, have been simulated to investigate the validity and applicability of the proposed 3D nonlinear timber model. These simulations confirmed that for all practical purposes the developed constitutive model for timber maybe considered as an acceptable and accurate modelling approach. Good agreement was seen between the calculated and the measured values for two different examples investigated here. The proposed FE model was able to predict the overall response of the hybrid timber beams under bending tests. The highest difference between numerical and experimental ultimate load-bearing capacities for the hybrid beams was only around 5%.

Further work is still to be done in order to introduce some other effects concerning the behaviour of timber material as damage induced anisotropy and moisture effects.

Conflict of interest

None.

References

[1] M. Khelifa, Numerical analysis of damage evolution of 3D timber-steel hybrid beams in bending. WCTE 2016-World Conference on Timber Engineering, August 22-25, 2016, Vienna, Austria.
[2] A. Tabiei, J. Wu, Three-dimensional nonlinear orthotropic finite element material model for wood, Compos. Struct. 50 (2000) 143–149.
[3] G.R. Johnson, J.M. Hoegfeldt, U.S. Lindholm, A. Nagy, Response of various metals to large torsional strains over a large range of strain rates - part 1: ductile metals, J. Eng. Mater. Technol. 105 (1) (1983) 42–47.
[4] A. Reiterer, S.E. Stanzl-Tschegg, Compressive behaviour of softwood under uniaxial loading at different orientations to thee grain, Mech. Mater. 33 (2001) 705–715.
[5] M. Oudjene, M. Khelifa, Elasto-plastic constitutive law for wood behaviour under compressive loadings, Constr. Build. Mater. 23 (11) (2009) 3359–3366.
[6] V.L. Tagarielli, V.S. Deshpande, N.A. Fleck, C. Chen, A constitutive model for transversely isotropic foams, and its application to the indentation of balsa wood, Int. J. Mech. Sci. 47 (2005) 666–686.
[7] R. Hill, A theory of the yielding and plastic flow of anisotropic materials, Proc. R. Soc. London A193 (1947) 281–297.
[8] V.S. Deshpande, N.A. Fleck, M.F. Ashby, Effective properties of the octet-truss lattice material, J. Mech. Phys. Solids 49 (8) (2001) 1747–1769.
[9] J.C.J. Schellekens, R. De Borest, The use of the Hoffman yield criterion in finite element analysis of anisotropic composites, Comput. Struct. 37 (6) (1990) 1087–1096.
[10] O. Hoffman, The brittle strength of orthotropic materials, J. Compos. Mater. 1 (1967) 200–206.
[11] B.H. Xu, M. Taazount, A. Bouchaïr, P. Racher, Numerical 3D finite element modelling and experimental tests for dowel-type timber joints, Constr. Build. Mater. 23 (2009) 3043–3052.
[12] W. Winter, K. Tavoussi, T. Pixner, F.R. Parada, Timber-steel-hybrid beams for multi- storey buildings. World Conference on Timber Engineering WCTE, New Zealand, 2012.
[13] A. Hassanieh, H.R. Valipour, M.A. Bradford, Experimental and numerical study of steel-timber composite (STC) beams, J. Constr. Steel Res. 112 (2016) 367–378.
[14] R. Gutkowski, K. Brown, A. Shigidi, J. Natterer, Laboratory tests of composite wood– concrete beams, Constr. Build. Mater. 22 (2008) 1059–1066.
[15] M. Oudjene, E.M. Meghlat, H. Ait-Aider, P. Lardeur, M. Khelifa, J.-L. Batoz, Finite element modelling of the nonlinear load-slip behaviour of full-scale timber-to-concrete composite T-shaped beams, Compos. Struct. 196 (15 July 2018) 117–126.
[16] Abaqus. Theory manual. Version 6.14. Providence, RI: Dassault Systèmes Simulia Corp., 2016.
[17] K. Saanouni, K. Nesnas, Y. Hammi, Damage modelling in metal forming processes, Int. J. Damage Mech. 9 (3) (2000) 196–240.
[18] A. Khennane, M. Khelifa, L. Bleron, J. Viguier, Numerical modelling of ductile damage evolution in tensile and bending tests of timber structures, Mech. Mater. 68 (2014) 228–236.
[19] J.-L. Chaboche, G. Cailletaud, Integration methods for complex plastic constitutive equations, Comput. Methods Appl. M 133 (1996) 125–155.
[20] J.C. Simo, T.J.R. Hughes, Computational Inelasticity, Springer, New York, 1998.
[21] AS/NZS 2098.2. Methods of Test for Veneer and Plywood – Bond Quality of Plywood, 2012.
[22] AS/NZS 3679.1. Hot-Rolled Bars and Sections, 2010.